Nanocomposites of Styrene–Butadiene Rubber and Synthetic Anatase Obtained by a Colloidal Route and Their Photooxidation

Tatiane M. Arantes,[1] Edson R. Leite,[1] Elson Longo,[2] Emerson R. Camargo[1]

[1]*LIEC-Interdisciplinary Laboratory of Electrochemistry and Ceramics, Department of Chemistry, UFSCar-Federal University of São Carlos. Rod. Washington Luis km 235, CP 676, São Carlos 13565-905, SP, Brazil*
[2]*Chemistry Institute of Araraquara, UNESP-São Paulo State University, Rua Francisco Degni, CP 355, Araraquara 14801-907, SP, Brazil*

Received 15 December 2008; accepted 29 January 2009
DOI 10.1002/app.30144
Published online 17 April 2009 in Wiley InterScience (www.interscience.wiley.com).

ABSTRACT: Photodegradable styrene–butadiene rubber (SBR)/TiO_2 nanocomposites were prepared by a colloidal route through the simple mixing of a commercial polymer latex and synthetic anatase nanoparticles. Stable colloids of pure anatase TiO_2 nanoparticles with an average diameter of 7 nm were prepared by a solvothermal route from the hydrolysis of titanium alkoxide by hydrogen peroxide in the presence of oleic acid. The photocatalytic degradation of the SBR–TiO_2 nanocomposites was carried out in ambient air at room temperature under a UV lamp and was monitored by Fourier transform infrared and UV–visible spectroscopies and differential scanning calorimetry. The results show that the SBR–TiO_2 nanocomposites were photocatalytically degraded under UV light, which indicate that the butadiene chains in the nanocomposite were oxidized during UV irradiation. Thermal analysis measurements indicated that crosslinking reactions occurred. The presence of anatase TiO_2 nanoparticles was found to accelerate the photocatalytic process, and the degradation mechanism was similar to that of the pure SBR polymer.
 J Appl Polym Sci 113: 1898–1904, 2009

Key words: colloids; degradation; elastomers; nano-composites; rubber

INTRODUCTION

Numerous efforts have focused on the search for new materials with lower costs, greater durability, and especially, lower environmental impact. In this sense, nanotechnology has become the focus of many research groups worldwide.[1] The term *nanocomposite* was introduced by Roy et al.[2] in 1984 to designate a particular composite material that contains at least one component of nanometric size. On this scale, nanofillers promote improvements in mechanical, thermal, and physicochemical properties when compared to pure polymers or traditional polymer-based microcomposites. The key point is the total interface area between these fillers and the polymeric matrix, which is much larger in nanocomposites, even when minor amounts of nanoparticles are inserted. Moreover, because of the low mass content of inorganic nanofillers, the processability and density of nanocomposite materials are not affected. Currently, the processability can sometimes increase when nanoparticles are introduced, and because of the small size of these particles, the scattering of visible light does not occur; this results in a material with optical transparency.[3]

The industrial sector rapidly identified the commercial advantages of using nanocomposites with greater mechanical strength; better optical, magnetic, or electrical properties; and higher thermal stability[4–7] and with maintained or improved processing characteristics of polymers.[8] The most popular class of nanocomposites studied are still those obtained from the insertion of modified organophilic clays, usually montmorillonite, with the aim of improving the thermal and mechanical properties and sometimes doubling the tensile modulus and strength without the sacrifice of impact resistance.[9–13] Other applications have focused on more efficient gas-barrier materials[6,14–16] or short-fire features.[17] However, if organophilic clays become popular nanofillers, there is a vast range of other nanospecies that can be used to obtain a different family of nanocomposites, including applications that involve technological applications of the intrinsic properties of synthetic nanoparticles in fields other than those restricted to mechanical performance. For instance, a recent

Correspondence to: E. R. Camargo (camargo@ufscar.br).
Contract grant sponsor: Fapesp-Fundação de Amparo à Pesquisa do Estado de São Paulo through CMDMC/Cepid-Multidisciplinary Center for Development of Ceramic Materials.
Contract grant sponsor: CNPQ-Conselho Nacional de Desenvolvimento Científico e Tecnológico (Brazil); contract grant number: 555644/2006-5.

report[18] described the formation of a luminescent nanocomposite through the incorporation of ZnS nanoparticles doped with manganese into the matrix of poly(methyl methacrylate). The literature also contains several references to the use of TiO_2,[19] SnO_2,[19] and SiO_2[20] nanoparticles, fibrous silicates, and hydroxide sheets, including those synthesized by hydrothermal processing.[21] Other examples are the synthesis of polymers with magnetic properties through the incorporation of ferrites, such as γ-Fe_2O_3 or Fe_3O_4, and the fabrication of solar cells with CdSe nanocomposites in a polymeric matrix.[22]

The most popular polymeric materials studied are still nylon and some thermoplastics materials, but little attention has been paid to the fabrication of elastomeric nanocomposites. Natural rubber is sometimes studied because of the environmental benefits of using renewable resources,[23] but there are numerous applications, mainly in the automotive sector, in which only synthetic rubbers can be used. Styrene–butadiene rubber (SBR) is a well-known commercial elastomeric polymer used in the production of a wide range of products, from shoes to flexible fuel tubes, from the construction industry to the transport sector.

In this study, we were interested in preparing nanocomposites based on the commercial polymer SBR produced on an industrial scale in a latex form through the insertion of functionalized synthetic nanoparticles (titanium oxide) with controlled size and shape and sharp size distributions. All of these nanoparticles were synthesized through nonaqueous solution routes under mild conditions of temperature and pressure. We obtained spherical nanoparticles of titanium oxides with an average diameter of 7 nm and with a sharp size distribution. The nanocomposites prepared from the mixture of these nanoparticles showed high photocatalytic sensitivity.

EXPERIMENTAL

All of the chemicals used in this study were of analytical grade and were used as received with no further purification. The water used here was deionized through a Millipore Elix-3 (Billerica, MA) purification system.

Synthesis of the titanium oxide nanoparticles

Nanoparticles of TiO_2 were prepared by the method described originally by O'Brien et al.[24] by the dissolution of 0.185 mL of titanium(IV) isopropoxide (97%, Merck, Darmstadt, Germany) in 30 mL of diphenyl ether (99.0%, Merck) in the presence of oleic acid (99.0%, Merck). Titanium alkoxide was added under an inert atmosphere to prevent premature hydrolysis of the alkoxide, and the nominal titanium concentration in this solution was 0.02 mol/L. An aqueous solution of hydrogen peroxide (30%, Sinth, São Paulo, Brazil) was injected into the system at 70°C under stirring to promote the controlled hydrolysis of the titanium alkoxide (H_2O_2 : Ti = 8 : 1). The flasks were kept at 120°C for 12 h, after which the nanoparticles were isolated by centrifugation, washed with hexane, and dried.

Nanocomposite synthesis

Anatase TiO_2 nanoparticles were dispersed in water (0.2%) with the addition of 0.1 mol/L dodecylbenzenesulfonic acid (DBSA) as a surfactant, added to the SBR colloidal lattice dispersions, and homogenized for 1 h. The SBR lattices with TiO_2 nanoparticles were then dried with Petri dishes in an air circulation oven at 50°C for several hours and then deployed as self-sustained nanocomposite films.

Characterization

Powder X-ray diffraction (XRD) patterns of the solids were recorded at room temperature with a Rigaku DMax 2500PC (Tokyo, Japan) diffractometer with Cu Kα radiation. The XRD patterns were collected in the 2χ range 10–110° with a scan step of 0.02° and a step time of 1 s. The crystallographic domain (crystalline size) of the TiO_2 nanopowders was determined for the most intense peak (101) planes of the TiO_2 pattern with Scherrer's formula.[25] The nanocomposites were analyzed by infrared absorption spectroscopy with a Fourier transform infrared spectrometer (Bruker EQUIXOX 55, Ettlingen, Germany) with an attenuated total reflectance accessory (ZnSe monocrystal). The spectra were collected at room temperature in the range 650–4000 cm^{-1}, with 32 scans and 4 cm^{-1} of resolution. Absorption transmittance spectra for the nanocomposites were obtained with a Varian model Cary 5G (Palo Alto, CA) spectrophotometer in the range 200–800 nm at a scan rate of 1 nm/s. The nanoparticle morphology was done with a Carl Zeiss Supra 35VP (Oberkochen, Germany) high-resolution field-emission gun coupled to a scanning/transmission electron microscope. Differential scanning calorimetry (DSC) measurements were taken with a Netzsch Phoenix 204 (Exton, PA) calorimeter in the range −100 to 200°C at a heating rate of 20°C/min.

Photodegradation

Square samples with an area of 2 cm^2 and a thickness of 0.5 mm were prepared from the nanocomposite films containing different amounts of TiO_2 nanoparticles. These samples and one control sample (without nanoparticles) were placed in a dark box, which was set at distance of 10 cm from the UV source to perform the photodegradation reactions. The

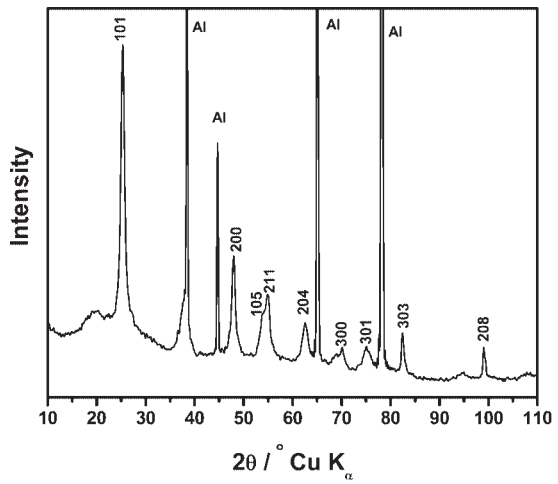

Figure 1 XRD pattern of TiO_2 with oleic acid (OLA) as surfactant with ratio of 1 Ti : 3 OLA. Al indicates the aluminum substrate.

radiation used in this experiment was obtained with a medium-pressure mercury vapor lamp (Osram, HQL 400) with output without a protection bulb.

RESULTS AND DISCUSSION

Synthesis of the TiO_2 nanoparticles

Recently, O'Brien et al.[24] proposed a sol–gel technique to prepare oxide nanoparticles from the hydrolysis of an appropriate alkoxide. In our case, we used titanium(IV) isopropoxide diluted in diphenyl ether. Unlike other forms of synthesis in organic media, where the solvent acts as a reactant, in this route, diphenyl ether is only the apolar medium for the formation of inverse micelles of oleic acid. Equation (1) shows the proposed reaction for formation through the action of the hydrogen peroxide oxidizing agent:

$$\mathrm{M{-}OR}_{n(l)} + \mathrm{H_2O_{2(aq)}} \longrightarrow \mathrm{MO}_{(s)} + \mathrm{nROH}_{(l)} + \mathrm{H_2O}_{(l)} \quad (1)$$

where the notation $(_l)$, $(_s)$ and $(_{aq})$ means liquid state, solid state, and aqueous media, respectively.

The role played by oleic acid is remarkable because the crystallization occurs inside the inverse micelle. It is, therefore, crucial to use correct amounts of oleic acid to ensure precise control of the shape and phase purity of the final compounds; mainly, one should consider the active role played by the surfactant molecules in the formation of inverse micelles. Pure anatase was only crystallized when a correct molar ratio of 1 Ti : 3 oleic acid was used (Fig. 1), but larger and smaller amounts of oleic acid resulted in a mixture of rutile and anatase. First, there was a dependence between the crystalline phase and the titanium oxide particle size, which benefited the anatase phase for small crystals up to 30 nm.[26] Second, the polar core of the inverse micelles also contained water from the hydrogen peroxide, which pushed the system to form nanoparticles with smaller volumes than those found inside the micelles.[27]

All the peaks observed in the X-ray pattern of Figure 1 were attributed to anatase phase, in accordance with the JCPDS card (Joint Committee on Power Diffraction standards) 21-1272. Several peaks from the aluminum sample holder were also observed and are shown in Figure 1. Crystallographic coherence domains (the size of the crystallite) were estimated with Scherrer's equation for different directions. An average crystallite size of 8 nm was obtained, but the values calculated for the different crystallographic orientations were also near to 8 nm, which indicated a spherical symmetry.

These particles were also characterized by field-emission gun scanning/transmission electron microscopy (FEG-STEM) to determine the morphology of the particles (Fig. 2). This image showed almost uniformly spherical nanoparticles with an average size of 7 nm, which was consonant with the values estimated by Scherrer's equation. Although the numbers were not exactly the same, one must consider the differences between the FEG-STEM and XRD techniques and their fundamental phenomena. Crystallite sizes are sometimes much smaller than those observed by electronic microscopy, which indicates that particles are formed through the joining of small blocks. However, in our case, the values were consistent with respect to shape and size, and most importantly, we concluded that each nanoparticle formed inside a micelle was a single crystal. Interestingly, the nanoparticles depicted in Figure 2 were located at approximately the same distance from each other. This uniform spatial arrangement of nanoparticles indicated that their surfaces were coated by oleic acid. This steric effect is beneficial for a self-assembling system, and it was this

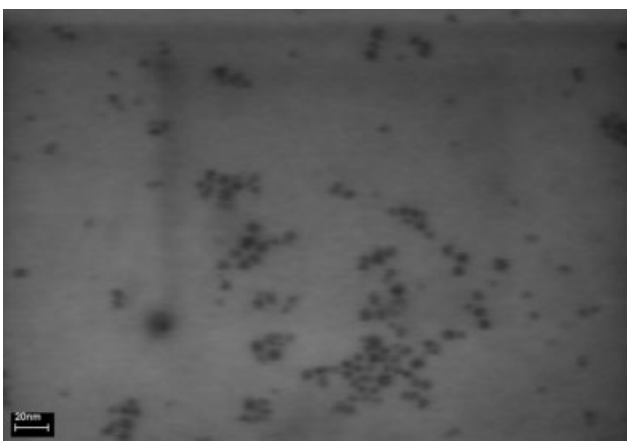

Figure 2 FEG-STEM micrograph of TiO_2 with oleic acid (OLA) as a surfactant in the mole ratio 1 Ti : 3 OLA.

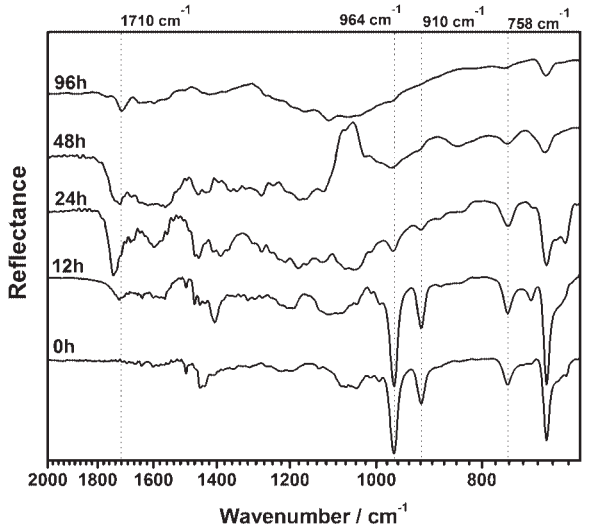

Figure 3 Fourier transform infrared image of the SBR–TiO_2 (0.2%) nanocomposites with DBSA as a surfactant, illuminated with a 400-W mercury lamp for different lengths of time.

hydrophobic layer of oleic acid that stabilized the colloidal particles in the apolar medium but resulted in water-insoluble particles.

To obtain stable aqueous colloidal dispersions, the hydrophilic nature of the nanoparticles had to be modified. To this end, aqueous solutions of DBSA were prepared, to which the TiO_2 nanoparticles were added, and the system was stirred for 1 h at room temperature. This procedure resulted in stable aqueous colloidal dispersions of the TiO_2 nanoparticles.

SBR and TiO_2 nanocomposites

Nanocomposites can be prepared by several methods, including *in situ* polymerization, melting routes, mechanical extrusion, and solution processing.[11] Although all these techniques have been widely and successfully applied to prepare nanocomposites of several compositions, our SBR nanocomposites were prepared by the colloidal route. This method offers the advantage of combining the processing flexibility of single mixtures with nearly molecular homogeneity. With this procedure, colloidal dispersions of the hydrophilic TiO_2 modified with DBSA were added to the commercial aqueous colloidal dispersions of SBR lattices and homogenized at room temperature. Self-sustained nanocomposite films were prepared easily from the solvent evaporation. During this stage, the SBR colloids agglutinated, and the TiO_2 nanoparticles were trapped in this process, maintaining their original homogeneity; this resulted in SBR nanocomposite films containing 0.2% TiO_2 nanoparticles.

These nanocomposites were exposed to UV light for different time intervals up to 96 h, and their attenuated total reflectance infrared spectra are shown in Figure 3. Typical frequencies of TiO_2 at 452 and 1103 cm^{-1} [28] were not visible, probable because of the low content. The carbonyl absorption frequency close to 1710 cm^{-1} was absent from the pure polymer but appeared after exposure to UV light. The formation of these carbonyl groups was attributed to the oxidation of the polymer in the presence of TiO_2 nanoparticles, which indicated the photocatalyzed degradation of the SBR matrix, similar to that observed in TiO_2–polystyrene nanocomposites.[29] It is also well known that titanium oxide produces photogenerated oxidant species; this leads to a much faster degradation of the polymer than when pure polymer or composites with different oxides, such as silicon or zinc oxides, are exposed to UV radiation. Figure 4 illustrates several reactions that occurred simultaneously but were determined by the absorption of one photon by the oxide nanoparticles. Photocatalytic polymer degradation was triggered by active oxygen species, such as $O_2^{\bullet -}$, $^{\bullet}HOO$, and $HO^{\bullet}$, which were formed on the surface of the TiO_2 nanoparticles. These active oxygen species attacked the polymer chain, removing the hydrogen atoms and forming radical carbon neighbors successively until chain cleavage occurred.[29]

Figure 3 also shows that the bands associated with *trans*-1,4-butadiene (at 960 cm^{-1}) and 1,2-butadiene (at 910 cm^{-1}) diminished, whereas the carbonyl bands (at 1710 cm^{-1}) increased simultaneously, which suggested that the double bonds of butadiene groups were oxidized by the species generated on the TiO_2 nanoparticles. Obviously, benzene rings could have also absorbed UV light and gradually formed macromolecular radicals. However, no kinetic change was observed in the aromatic band at 758 cm^{-1}, whereas the butadiene bands decreased under exposure to UV radiation; this suggested a selective kinetic attack of the oxidizing agent on the double bond. The benzene band appeared to be modified only after 48 h of exposure, when the butadiene bands disappeared from the spectrum.

Mechanism of nanocomposite photodegradation

Several research groups have engaged in studies of the photocatalyzed degradation of polymers

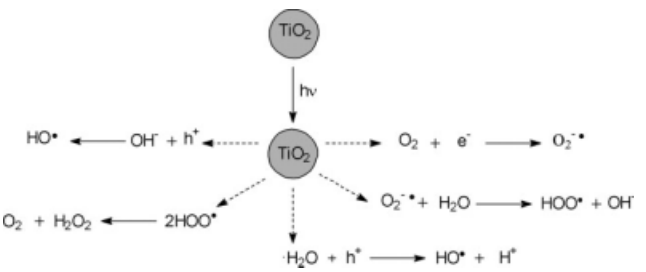

Figure 4 Schematic diagram of active oxygen species generated on the surface of the TiO_2 nanoparticles.[29] hv, one energy foton.

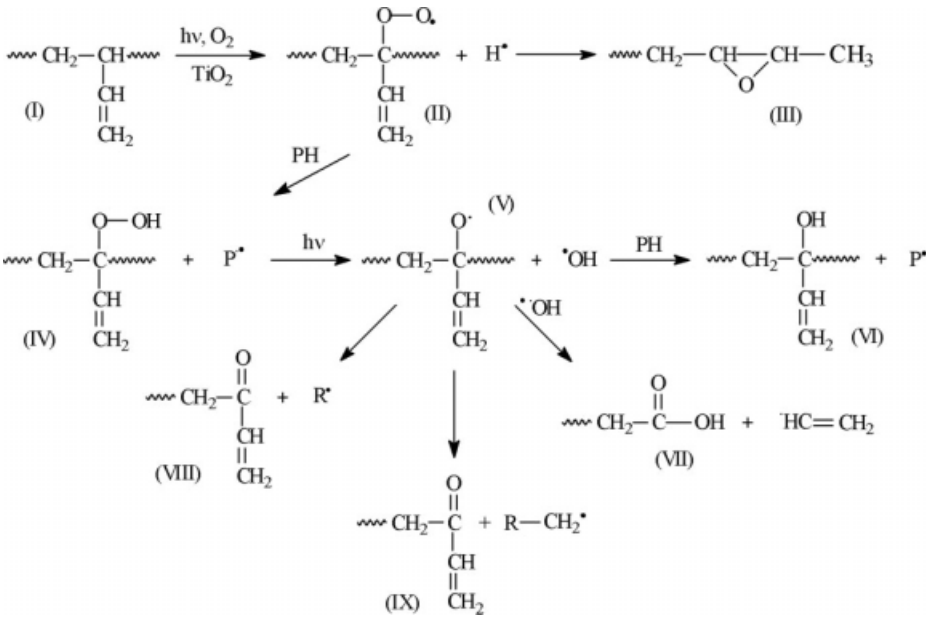

Figure 5 Butadiene chain photodegradation reactions.

containing polybutadiene groups, such as nitrile rubber,[30] butadiene rubber,[31] acrylonitrile–butadiene–styrene,[31,32] and SBR.[33,34] It has been suggested that polymer degradation is mainly controlled by the reactivity of 1,2-butadiene and of *cis*- and *trans*-1,4-butadiene isomers. These three isomers appear to be degraded by similar mechanisms, but 1,2-butadiene seems to form the radical more readily than 1,4-butadiene because of the existence of a labile hydrogen in the tertiary carbon. The degradation, process depicted in Figure 5, begins when titanium oxide nanoparticles absorb a photon, thereby catalyzing the formation of the peroxide alkyl radical through the elimination of a labile hydrogen. This radical can recombine with the double bonds of butadiene groups and form an epoxy radical that propagates the degradation to other double bonds. On the other hand, instead of forming an epoxy intermediate, the peroxide radical can capture a hydrogen atom to produce an alkyl hydroperoxide radical and propagate the degradation through the formation of carbonyl groups in several ways; this decreases the concentration of double bonds. Apparently, the intensity of the 1,2-butadiene peak at 910 cm^{-1}, shown

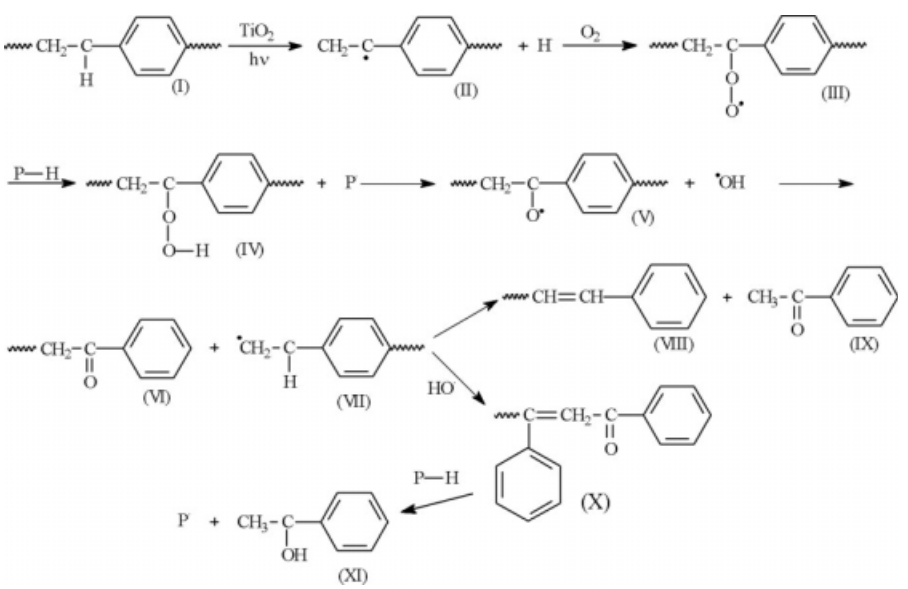

Figure 6 Formation reaction of αβ-unsaturated carboniles in a styrene chain.

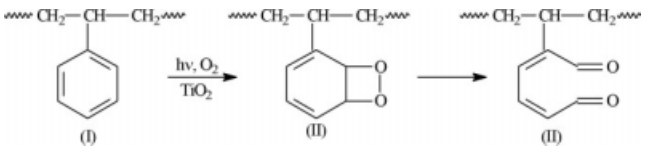

Figure 7 Reactions to divide the benzene ring in the styrene chain.

in the infrared spectra of Figure 3, decreased faster than the 1,4-butadiene peak at 960 cm^{-1}, in accordance with this discussion.

The spectra in Figure 3 also show that the aromatic rings of styrene groups were almost completely preserved until the butadiene groups were totally oxidized, as indicated by the 758-cm^{-1} band of the aromatic ring, which was modified only after 48 h of exposure to UV radiation, as discussed earlier. However, the presence of a small peak at 1672 cm^{-1} in the spectrum of the nanocomposite exposed for 24 h was strong evidence of the formation of α,β-unsaturated carbonyl byproducts from the oxidation of the styrene units. This mechanism is illustrated in Figure 6. First, a photon was transferred to the tertiary carbon near the aromatic ring; this formed a hydroperoxide radical that propagated the degradation and produced the α,β-unsaturated carbonyl groups at this carbon and preserved the aromatic ring.

The intensity of the aromatic band at 758 cm^{-1} decreased only after 96 h of irradiation; this indicated the oxidation of this group. According to Zan et al.,[35] aromatic rings are probably oxidized to aldehydes, as shown in Figure 7. These aldehydes can also be further oxidized photocatalytically because of the action of active oxygen species produced on the surface of nanoparticles, which leads to the degradation of the aromatic rings of styrene groups.

Jubete et al.[36] used the ratio of the intensity of the carbonyl band (at 1715 cm^{-1}) to the aromatic skeletal vibration (1492 cm^{-1}) to evaluate the photodegradation efficiency, which is referred to as the *carbonyl index*. This number estimates the oxidation degree of the material that is proportional to the intensity of the carbonyl band relative to an internal reference. The value calculated for the nanocomposites with 0.2% TiO_2 (4.65) was almost twice that of the carbonyl index calculated for the nanocomposite with only 0.02% nanoparticles (2.90); this indicated that the photodegradation efficiency was directly related to the amount of nanosized titania added. For comparison purposes, the carbonyl index of pure SBR was of 1.02 after 96 h of exposition.

Figure 8 shows the transmittance curves in the UV–visible region of the degraded TiO_2–SBR nanocomposites and the curves of the pure SBR film and fresh nanocomposite without exposure. Note that the transmittance increased steadily as a function of

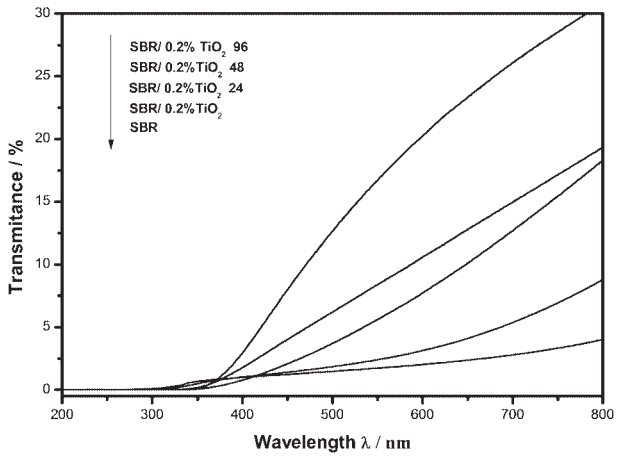

Figure 8 UV–visible spectra of pure SBR and nanocomposite SBR containing 0.2% TiO_2 and DBSA as a surfactant before illumination and monitored photodegradation.

exposure time; this indicated a correlation between the degree of degradation and the transparency. The increased transparency was attributed to oxidation of the double bonds of the butadiene dienes. These double bonds conferred greater opacity to the polymer, and their oxidation made the polymer more transparent. All of the nanocomposites became insoluble in organic apolar solvents after exposure to UV radiation; this indicated a high degree of reticulation promoted by photodegradation. It appeared that prolonging the photodegradation time caused the polymer to become more rigid and increased the glass-transition temperature (T_g). Crosslinking reactions probably occurred between the polymer chains during the degradation process. This process caused the different chains to be linked by covalent bonds, so the material became stiffer and less soluble in organic solvents. These reactions occurred particularly in the chains containing α,β-unsaturated carbonyls. Figure 9 shows the DSC curves of the pure polymer

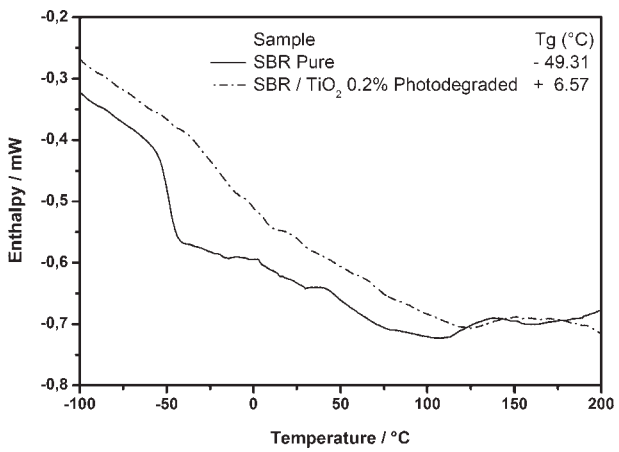

Figure 9 DSC curves for the pure SBR and SBR–TiO_2 nanocomposites after 300 h of photodegradation.

and of the nanocomposite after 300 h of exposure. In the first curve, T_g was clearly observed at −49.3°C, characterized by the second-order transition, which showed a modification in the base line. On the other hand, the degraded nanocomposite showed a typical curve of vulcanized rubber, without a visible transition temperature. Its T_g was calculated as 6.5°C, which was almost 50°C higher than that calculated for the pure polymer.

CONCLUSIONS

Nanoparticles of pure TiO_2 anatase structure were synthesized by a solvothermal methodology; this resulted in spherical single crystalline particles with an average diameter of 7 nm and a sharp size distribution. The nanoparticles synthesized by this method could be dissolved in water only with appropriate surfactants. Nanocomposites of SBR and TiO_2 were synthesized by the colloidal route, by a simple mixture of aqueous nanoparticle dispersions and commercial SBR lattices. Anatase nanoparticles were found to catalyze the photodegradation of the SBR matrix through the inherent mechanism of the pure polymer. However, the nanocomposites were degraded about four times faster than the pure polymer when exposed to UV radiation. These results indicate that the presence of oxide nanoparticles can catalyze polymer photodegradation without, however, affecting the degradation mechanism.

The authors give special thanks to Nitriflex.

References

1. Nam, P. H.; Maiti, P.; Okamoto, M.; Usuki, T.; Hasegawa, N.; Usuki, A. Polymer 2001, 42, 9633.
2. Roy, R.; Komarneni, S.; Roy, D. M. Mater Res Soc Symp Proc 1984, 32, 347.
3. Alexandre, M.; Dubois, P. Mater Sci Eng 2000, 28, 1.
4. Winey, K. I.; Vaia, R. A. MRS Bull 2007, 32, 314.
5. Oberdisse, J. Mater Sci 2005, 1.
6. Esteves, A. C. C.; Timmons, A. B.; Trindade, T. Quim Nova 2004, 27, 798.
7. Wiebeck, H.; Harada, J. Plásticos de Engenharia; Artiliber: São Paulo, Brazil, 2005.
8. Krishnamoorrti, R.; Vaia, R. A. ACS Symp Ser 2001, 804, Chap 1.
9. Usuki, A. U.S. Pat. 4,889,885 (1989).
10. Baur, J.; Silverman, E. MRS Bull 2007, 32, 328.
11. Gao, F. Mater Today 2004, 7, 50.
12. Chen, B.; Liu, J.; Chen, H.; Wu, J. Chem Mater 2004, 16, 4864.
13. Ishida, H. Chem Mater 2000, 12, 1260.
14. Wang, Z.; Pinnavaia, T. J. Chem Mater 1998, 10, 3768.
15. Lan, T. Chem Mater 1994, 6, 573.
16. Liang, Y. Polym Test 2005, 24, 12.
17. Beyer, G. Plast Addit Compd 2002, 22.
18. Althues, H. Chem Mater 2006, 18, 1068.
19. Schnitzler, D. C.; Zarbin, A. J. G. J Braz Chem Soc 2004, 15, 378.
20. Rong, M. Z.; Zhang, M. Q.; Zheng, Y. X.; Zeng, H. M. Polymer 2001, 42, 3301.
21. Di Maggio, R.; Fambri, L.; Mustarelli, P.; Campostrini, R. Polymer 2003, 44, 7311.
22. Huynh, W. U.; Dittmer, J. J.; Alivisatos, A. P. Science 2002, 295, 2425.
23. Valadares, L. F.; Leite, C. A. P.; Galembeck, F. Polymer 2006, 47, 672.
24. O'Brien, S.; Brus, L.; Murray, C. B. J Am Chem Soc 2001, 123, 12085.
25. Rashad, M. M.; Baioumy, H. M. J Mater Proc Tech 2008, 195, 178.
26. Billik, P.; Plesch, G. Mater Lett 2007, 63, 1183.
27. Zhang, W.; Qiao, X.; Chen, J. Mater Chem Phys 2008, 109, 411.
28. Zhang, L.; Liu, P.; Su, Z. Polym Degrad Stab 2006, 91, 2213.
29. Zan, L.; Tian, L.; Liu, Z.; Peng, Z. Appl Catal A 2004, 264, 237.
30. Adam, C.; Lacoste, J.; Lemaire, J. Polym Degrad Stab 1990, 27, 85.
31. Piton, M.; Rivaton, A. Polym Degrad Stab 1997, 55, 147.
32. Adeniyi, J. B.; Kolawole, E. G. Eur Polym J 1984, 20, 43.
33. Bousquet, J. A.; Fouassier, J. P. Eur Polym J 1987, 23, 367.
34. Adam, C.; Lacoste, J.; Lemaire, J. Polym Degrad Stab 1989, 26, 269.
35. Zan, L.; Wang, S.; Fa, W.; Hu, Y.; Tian, L.; Deng, K. Polymer 2006, 47, 8155.
36. Jubete, E.; Liauw, C. M.; Jacobson, K.; Allen, N. S. Polym Degrad Stab 2007, 92, 1611.